

Chemical Science

Accepted Manuscript

This article can be cited before page numbers have been issued, to do this please use: E. I. Stern, K. A. Thurman, F. Brito dos Santos and P. A. Kempler, *Chem. Sci.*, 2026, DOI: 10.1039/D6SC00974C.



This is an Accepted Manuscript, which has been through the Royal Society of Chemistry peer review process and has been accepted for publication.

Accepted Manuscripts are published online shortly after acceptance, before technical editing, formatting and proof reading. Using this free service, authors can make their results available to the community, in citable form, before we publish the edited article. We will replace this Accepted Manuscript with the edited and formatted Advance Article as soon as it is available.

You can find more information about Accepted Manuscripts in the [Information for Authors](#).

Please note that technical editing may introduce minor changes to the text and/or graphics, which may alter content. The journal's standard [Terms & Conditions](#) and the [Ethical guidelines](#) still apply. In no event shall the Royal Society of Chemistry be held responsible for any errors or omissions in this Accepted Manuscript or any consequences arising from the use of any information it contains.

Metal Cations Promote Coupled-Ion-Electron Transfer During Deposition and Corrosion

E. I. Stern, K. A. Thurman, F. Brito dos Santos, P. A. Kempler*

¹Department of Chemistry and Biochemistry and the Oregon Center for Electrochemistry,

University of Oregon, Eugene, OR, USA

*Correspondence: pkempler@uoregon.edu

Abstract:

During electrodeposition and corrosion reactions, dissolved metal ions transfer across the electrochemical double layer, undergoing changes in their solvation environment and oxidation state. The solvent reorganization during charge transfer is expected to increase with the charge density of the dissolved species, but the mechanistic pathway of cation (de)solvation remains poorly understood. Here, we have quantified the kinetics of underpotential deposition for two ions associated with rapid metal deposition kinetics: Cu²⁺ and Ag⁺, at site-defined Au(111) surfaces for deposition and corrosion. Both metal adsorbates exhibited reversible adsorption kinetics at low coverage and slow scan rates, along with a symmetric transfer coefficient, $\alpha \sim 1/2$, consistent with a single electron/ion transfer during the rate determining step. The standard rate constant for Ag⁺ transfer was within an order of magnitude of reported adiabatic electron transfer rate constants, and the kinetics of Cu²⁺ transfer were consistent with the rate determining step involving metal adsorption. The self-exchange rate for both Ag⁺ and Cu²⁺ transfer exhibited a reaction order of $\sim 2\alpha$ with respect to cation concentration, indicating that metal cations promote their own ion transfer step and a self-consistent mechanism involving solvent exchange prior to ion transfer is



proposed. Insights from this kinetic model could support improved additives for metal deposition in semiconductors, redox-flow battery electrolytes, and electrorefining processes for energy-critical metals.

Introduction:

Electrochemical deposition and corrosion of transition metals are a class of reactions fundamental for batteries, industrial refining of metals, and advanced manufacturing of semiconductor devices. The electrochemical corrosion and deposition of Cu^{2+} is used to refine nearly all Cu metal used in wiring, electronics, and plumbing; advanced embodiments of Cu and Ag deposition are used to form interconnects within nano- to micro-scale vias in most semiconductor devices.¹⁻³ Nevertheless, the elementary steps associated with aqueous deposition, particularly of multivalent species, remain poorly understood such that strategies to control deposition and corrosion are identified empirically.⁴ The microscopic steps associated with transferring a solvated ion across the electrified solid-liquid interface are generally made complicated by ill-defined electric fields, large solvation energies, and a poorly defined population of adsorbates and adsorption sites—collectively, these steps are referred to interfacial ion transfer, IIT.⁵⁻⁷ Resolving microscopic steps associated with metal IIT can clarify our understanding of the dynamic structure of electrified interfaces and provide a unifying theory for ion transfer reactions to connect with established theories of electron transfer.^{8,9}

The adsorption of a metal cation is an IIT reaction required for electrochemical deposition and should involve (in no particular order) electron transfer(s) to the cation, adsorption to a surface site, loss of the solvation shell, and reorganization of the local double layer structure. Conway claimed that the reduction of Cu^{2+} to Cu^+ is the rate determining step (RDS) for Cu deposition whereas Ag^+ IIT becomes the rate determining step for Ag deposition at high overpotentials.¹⁰ The



standard rate constants for Co^{2+} , Ni^{2+} , and Fe^{2+} deposition are 10^3 – 10^5 times less than those for Ag^+ and Cu^{2+} , which may be related to the fact that the former metals lack a stable +1 oxidation state.¹⁰ Gileadi noted the curiosities associated with high exchange current densities for metal deposition relative to the comparable rates of outer-sphere electron transfer and proposed a mechanism in which the free energy of the system is lowered through a gradual delocalized electron transfer from the metal to the solvated ion which lowers the energy for the stepwise removal of water molecules.¹¹ More recent simulations and experiments have suggested that aqueous Ag^+ may approach within a few angstroms of the surface before undergoing a rapid transfer enabled by favorable interactions between the Ag 5s orbital and a delocalized sp band from the metal.^{12,13} These findings provide insights into rapid kinetics for monovalent metal deposition but fail to resolve the more complex picture required for understanding the deposition and corrosion of multivalent metal ions.^{14–18}

Underpotential deposition (UPD) on site-defined Au surfaces is a well-suited system for addressing the complexities of interfacial ion transfer. UPD is a phenomenon where ions are adsorbed onto the surface at potentials more favorable compared to the standard reduction potential where the deposition would be expected. This phenomenon is caused by more favorable surface-adsorbate interactions compared to the adsorbate adsorbing on to itself. UPD is thus an inherently self-limiting process, and the surface coverage is a state function that can be easily controlled by the applied electrochemical potential. UPD on a wide variety of single crystal surfaces have well characterized surface phases and phase transitions.^{19–21} Cu and Ag UPD at Au(111) is a suitable model system to compare the mechanism for IIT for monovalent and divalent metal cations, as both metals have similar lattice constants and exhibit kinetic regions of quasireversible adsorption/desorption. Whereas Cu^{2+} can be repeatedly adsorbed/desorbed from the Au surface,



Ag participates in exchange with surface Au atoms which has previously hindered the characterization of Ag^+ adsorption.^{22,23}

Here, we conduct site-defined measurements of transition metal IIT kinetics for Ag^+ and Cu^{2+} at Au(111) in two non-coordinating electrolytes to develop a microscopic framework for metal deposition and corrosion. The use of an inert and well-defined Au(111) substrate for adsorption allowed kinetics to be quantified with a known number of active sites and a known coverage of adsorbed intermediates, neither of which are possible at a growing/corroding metal surface. Divalent Cu^{2+} adsorption is shown to be controlled by a single charge transfer step with a symmetric transfer coefficient and an adsorbed product. The reaction order of metal ion transfer was quantified with respect to the concentration of dissolved metals and the coverage of intermediates, indicating the presence of a multistep adsorption mechanism present even for elementary univalent ion transfer.

Experimental Methods:

Chemicals: Deionized water with a resistivity of 18.2 $\text{M}\Omega\text{ cm}$, DI H_2O , was obtained from a laboratory water purification system (Thermo Scientific Barnstead Nanopure). Perchloric acid (HClO_4 , 10.25 M, TraceMetal Grade) and sulfuric acid (H_2SO_4 96% aq, TraceMetal Grade) were obtained from Fisher Chemical, whereas silver perchlorate monohydrate (99.999% metals basis) and copper(II) oxide (99.99% trace metals basis) were obtained from Sigma-Aldrich. Silver perchlorate monohydrate and copper(II) oxide were used as sources of Ag^+ and Cu^{2+} , respectively, for all experiments.

Electrodes: Au(111) surfaces were prepared from thermally evaporated Au (4N) on titanium-coated glass slides (GOLD SEAL®, Electron Microscopy Sciences). Slides were cleaned



in an oxygen plasma for 15 min before being transferred to a thin-film deposition system (Angstrom Engineering). A 17 nm adhesion layer of Ti was deposited via electron beam evaporation followed by 200 nm of thermally evaporated Au. As-deposited Au electrodes were annealed under a butane flame and cooled in an Ar(g) stream before being transferred to cell environment. X-ray diffraction of these surfaces indicated that the surface was primarily oriented to expose the Au(111) surface after annealing (**Figure S1**) A flame-cleaned Pt wire (99.997% metals basis, Thermo-Scientific) served as the counter electrode. A high purity Ag wire (99.999%, Thermo-Scientific) or Cu wire (99.999%, Alfa Aesar) served as quasi-reference electrodes and were protected behind a fritted glass pipette filled with an electrolyte identical to that in the cell to avoid contamination. Quasi reference electrodes were checked against a mercury sulfate reference electrode in saturated potassium sulfate (MSE) after voltammetry experiments.

Electrochemistry: Glassware was cleaned in H₂SO₄ with a persulfate-based oxidizing agent (Alnochromix) for >24 h to remove trace contaminants and then boiled three times in DI H₂O. Solutions were purged under ultrahigh purity Ar (99.999%) for at least 15 minutes and kept blanketed with a gentle flow of Ar during experiments. Cu-containing solutions were prepared by dissolving CuO in HClO₄ and all Ag-containing solutions were prepared by dissolving AgClO₄·H₂O in HClO₄. All electrochemical data was collected on a Bio-Logic SP-300. Reported electrochemical potentials, E , are referenced to a mercury sulfate electrode (MSE) or the reversible potential for metal deposition at Cu or Ag (E_{rev}). E_{rev} for Cu was ~ -410 mV vs MSE for 1 mM CuO in 100 mM HClO₄ and E_{rev} for Ag was ~ -40 mV vs MSE for 1 mM AgClO₄ in 99 mM HClO₄. Stability of the Au(111) interface was checked by sweeping the potential at a scan rate (v) of 25 mV s⁻¹ until a steady electrochemical response was reached (3–10 cycles). For measurements on Cu adsorption kinetics, the potential was cycled repeatedly from 0.000–0.600 V vs E_{rev} at



various ν and the second cycle was used for analysis. For Ag UPD, the surface quality was confirmed using voltammetry at 25 mV s^{-1} and then the potential was stabilized at 0.300 V vs E_{rev} for 10 s before a series of linear sweeps were collected from $0.300\text{--}0.585 \text{ V}$ vs E_{rev} at various ν . For both Cu and Ag, ν was varied from 25 mV s^{-1} to 50 V s^{-1} , with high concentrations of adsorbates or supporting electrolyte requiring faster ν to observe the impact of kinetics.

Results:

Cyclic voltammetry of Cu^{2+} at Au(111)-textured electrodes in $\text{HClO}_4(\text{aq})$ yielded a broad adsorption wave from -0.40 to -0.15 V vs MSE with a sharp desorption wave from -0.20 to -0.05 V vs MSE, characteristic of UPD of Cu on Au(111) in $\text{HClO}_4(\text{aq})$ (**Figure 1a**).^{24,25} The current response from $E = -0.15$ to 0.00 V was equal and opposite for the scans in the negative and positive directions, consistent with a reversible adsorption process.



Cyclic voltammetry of Ag^+ at Au(111)-textured electrodes in $\text{HClO}_4(\text{aq})$ yielded a reversible adsorption peak between $E = 0.45\text{--}0.55$ V vs MSE, a broad, capacitive region from $E = 0.15\text{--}0.50$ V, and a sharp irreversible adsorption peak from $E = -0.05\text{--}0.05$ V; all cathodic charge

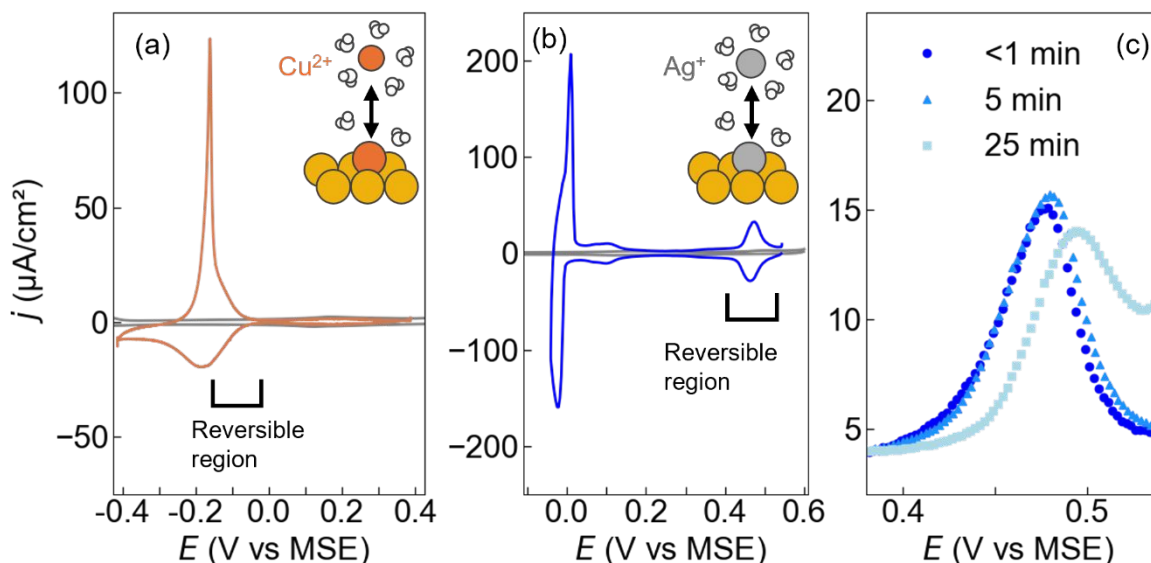


Figure 1: (a) Cyclic voltammetry of Cu UPD on Au(111) in 0.001 M $\text{Cu}(\text{ClO}_4)_2$ and 0.098 M HClO_4 (0.100 M ClO_4^-). (b) Ag UPD on Au(111) in 0.001 M AgClO_4 and 0.099 M HClO_4 (0.100 M ClO_4^-). The gray traces in (a) and (b) represent the CV of Au(111) in 0.100 M HClO_4 . (c) Cyclic Voltammetry of Ag UPD on Au(111) in a solution of 0.001 M AgClO_4 and 0.099 M HClO_4 (0.100 M ClO_4^-) as a function of time spent in solution. All scans were recorded at 25 mV/s and initially swept in the negative direction.

was balanced by commensurate desorption peaks and were qualitatively consistent with Ag UPD at Au(111) single crystals in $\text{HClO}_4(\text{aq})$ (**Figure 1b**).^{26,27} The total integrated charge from $E = -0.050$ to 0.550 V was $276 \mu\text{C cm}^{-2}$, which is consistent with the reported value for Ag^+ adsorption at Au(111) crystals from HClO_4 electrolytes and slightly greater than the theoretical value of $222 \mu\text{C cm}^{-2}$ for a close packed monolayer of Ag. We focused on potential regions yielding reversible and low coverage of adsorbates such that charge passed could be assigned to isolated adsorbates on a site-defined metal surface. The measured current density was normalized to scan rate, j/ν , and all potentials were measured against the equilibrium potential for bulk deposition/corrosion in the working electrolyte.



The stability of Au(111) surfaces in solutions containing Ag^+ was investigated using voltammetry and X-ray photoelectron spectroscopy (XPS). Following the scans for Ag UPD a positive potential shift for the charge in the reversible E region of < 5 mV was observed and XPS analysis revealed that < 3.5 % (as a ratio of $\text{Ag}/(\text{Ag}+\text{Au})$, **Table S1**) of the surface Au atoms had been replaced with Ag. After 20 min of potential cycling, the peak potential had shifted positively by > 20 mV, with > 10 % Ag present at the surface of the Au(111) electrode (**Figure 1c and Figure S2**). Further analysis was restricted to electrodes with low extents of Ag-Au alloying on the surface, $< 3\%$, such that most of the adsorption sites could be described by three-fold hollow sites coordinated with Au atoms. The peak binding energies for the remaining Ag (368.3 eV) detected in the Ag3d region were consistent with Ag (368.2 eV) metal rather than Ag^+ (e.g. AgCl, 367.4 eV).²⁸



The integrated charge in the potential range 0.15–0.39 V and 0.46–0.58 V vs E_{rev} for Cu and Ag, respectively (**Figure 2a**, **Figure 2d**, **Figure S3**), was normalized to the theoretical charge density of a full monolayer on Au(111) ($Q_{Cu}^* = -0.44 \text{ mC cm}^{-2}$, $Q_{Ag}^* = -0.22 \text{ mC cm}^{-2}$) to estimate metal coverage, θ_M (**Figure 2b**, **Figure 2e**, eq 1).

$$\theta_M(E) = \frac{1}{Q_M^*} \int_{E_i}^{E_f} \frac{j}{v} dE \quad (1)$$

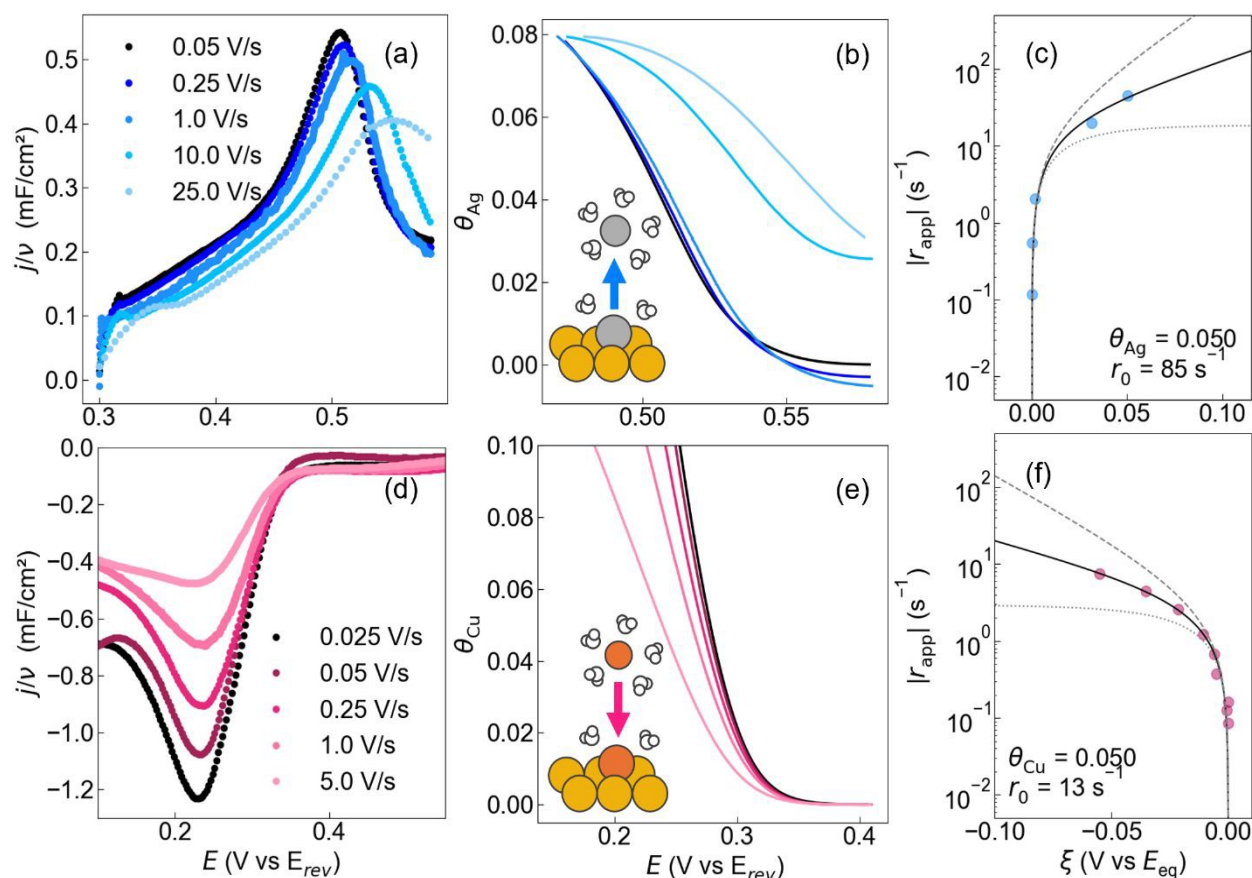


Figure 2: (a) LSV of Au(111) in 0.003 M AgClO₄ and 0.097 M HClO₄ (0.100 M ClO₄⁻) in the Ag UPD quasireversible region normalized to scan rate ($v = 0.05, 0.25, 1, 10, 25 \text{ V s}^{-1}$). (b) Scan rate dependent Ag coverage (θ_{Ag}). (c) Apparent interfacial ion transfer rate (r_{app}) of Ag⁺ as a function of surface overpotential (ξ) at $\theta_{Ag} = 0.05$. Markers represent individual trials and the transfer coefficient, α , was assumed to be 0.5 when fitting the data. Gray dotted and dashed lines represent an alternate fit with $\alpha = 0$ or $\alpha = 1$, respectively. (d) CV of Au(111) in 0.003 M Cu(ClO₄)₂ and 0.094 M HClO₄ (0.100 M ClO₄⁻) in the Cu UPD quasireversible region normalized to ($v = 0.025, 0.05, 0.25, 1.0, 5.0 \text{ V s}^{-1}$). (e) Cu coverage (θ_{Cu}) as a function of scan rate obtained by integrating the Cu UPD region. (f) r_{app} - ξ behavior for Cu²⁺ at $\theta_{Cu} = 0.05$.



At $\nu < 1.0 \text{ V s}^{-1}$ the current response of Ag^+ was linear with ν (**Figure S4**) and the peak potential was invariant with ν , both of which are consistent with reversible desorption kinetics. At $\nu > 1.0 \text{ V s}^{-1}$, a positive potential shift in the scan-rate-normalized current response was observed. The Cu^{2+} adsorption response began to shift negative at $\nu > 0.25 \text{ V s}^{-1}$. The apparent rate of metal IIT (r_{app}) was calculated using equation 2,

$$r_{\text{app}} = \frac{|j_{\text{M}}(E)|}{Q_{\text{M}}^*} \quad (2)$$

where $j_{\text{M}}(E)$ is the current density corrected for double layer charging in the absence of either dissolved Cu or Ag. Details on the methods used to correct for double layer charging are available for both species (**Supplementary Information, S2**). The dependence of the IIT rate on the surface overpotential, $\xi (E - E_{\text{eq}})$ —an expression of the difference between the applied electrode potential and the experimentally observed equilibrium potential for a given coverage—was fit to a generalized Butler-Volmer relationship assuming that the charge transferred during the RDS (**eq 3**)

$$r_{\text{app}} = r_0 \theta_{\text{M}}^{1-\alpha} (1 - \theta_{\text{M}})^{\alpha} \left(\exp\left[\frac{\alpha e \xi}{k_{\text{B}} T}\right] - \exp\left[\frac{-(1-\alpha) e \xi}{k_{\text{B}} T}\right] \right) \quad (3)$$

where α , e , k_{B} , T , and r_0 are the transfer coefficient, elementary charge, Boltzmann constant, temperature, and exchange rate, respectively (**Figure 2c**, **Figure 2f**). This method of analyzing scan-rate-dependent voltammetry data has previously been employed in studies on H adsorption on Pt(111), OH^* adsorption on Pt(111), and for Cu adsorption on Au(111).^{29–31} For all experimental conditions, the data was well described by assuming a consistent value for α of 0.5.

The exchange rate for Ag IIT increased from 28–173 s^{-1} for $[\text{Ag}^+] = 1$ to 10 mM, respectively when the total $[\text{ClO}_4^-]$ was 0.100 M. A similar trend was observed in electrolytes



containing 1.00 M ClO_4^- , with r_0 ranging from 30–470 s^{-1} over $[\text{Ag}^+] = 1\text{--}10$ mM (**Figure S5**). The apparent r_0 was constant for $\theta_{\text{Ag}} = [0.04\text{--}0.08]$, suggesting the kinetic model was appropriate (**Figure S6a**). Cu IIT at identical concentrations and coverages yielded more sluggish kinetics, with r_0 ranging from 4–35 s^{-1} and 5–70 s^{-1} in 0.100 and 1.00 M ClO_4^- , respectively (**Figure S7**).

To understand the interactions between divalent cations and divalent SO_4^{2-} , a common component of metal plating and refining baths, we additionally quantified the adsorption kinetics for Cu^{2+} in H_2SO_4 . Cu UPD at Au(111) surfaces in sulfate solutions yielded a characteristic set of

peaks associated with two distinct surface phases and a broad, quasireversible region at $E > 0.23$ V vs E_{rev} which was used for kinetic analysis (**Figure S8**). The total adsorbed charge prior to kinetically irreversible phase transitions was greater in H_2SO_4 electrolytes and so these samples were used to conduct stripping voltammetry data in a similar manner to Ag (**Figure S9**). For $\nu < 3$ V s^{-1} a single peak corresponding to the reversible region positive of the first phase transition was present (**Figure S9a**), for $\nu > 10$ V s^{-1} multiple peaks appeared around the region that charge equivalent to $\theta_{\text{Cu}} = 0.050$ remained on the surface (**Figure S9b**). At a surface coverage of 5%, $\theta_{\text{Cu}} = 0.050$ and 0.100 M SO_4^{2-} , the exchange rates measured from scans in the adsorption direction

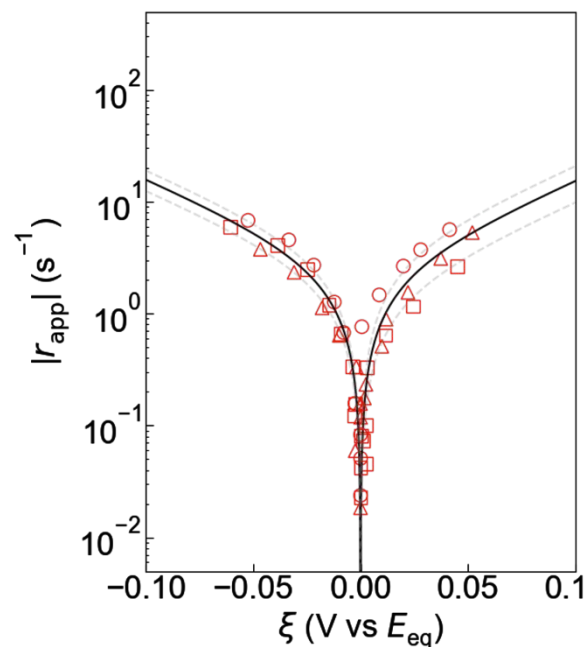


Figure 3: The apparent interfacial ion transfer rate (r_{app}) for 0.001 M Cu^{2+} in 0.100 M SO_4^{2-} as a function of ξ at $\theta_{\text{Cu}} = 0.05$. Each set of symbols represents one experiment in which both adsorption and desorption experiments were collected in the same cell with the same electrodes. The different markers represent the experimental repeats. The solid black line represents the averaged line of best fit, and the grey dashed lines represent one standard deviations of the fit.



($11 \pm 2 \text{ s}^{-1}$) and desorption direction ($11 \pm 4 \text{ s}^{-1}$) were in quantitative agreement (**Figure 3**, **Figure S6c**, **S7**) and slightly higher than the exchange rate for adsorption measured in 0.100 and 1.00 M ClO_4^- (**Figure S6b**, **Figure S7**).

Both Cu and Ag show an increase in the r_0 as the concentration of the respective metal cation increases as well as modest relationship between r_0 and the supporting electrolyte concentration (**Figure S5**, **Figure S7**). The reaction order, m_X , was described by

$$m_X = \partial \log(r_0) / \partial \log([X]) \quad (4)$$

where $[X]$ is the molarity of the species X . The change in r_0 with respect to $[\text{Ag}^+]$ is 0.78 ± 0.09 and 1.2 ± 0.07 in 0.10 and 1.00 M ClO_4^- , respectively. Similar m were measured for $\text{Cu}^{2+}(\text{aq})$: 0.99 ± 0.06 and 1.1 ± 0.1 at the same respective $[\text{ClO}_4^-]$ as well as 1.00 M $\text{HSO}_4^-/\text{SO}_4^{2-}$ ($m = 0.80$,

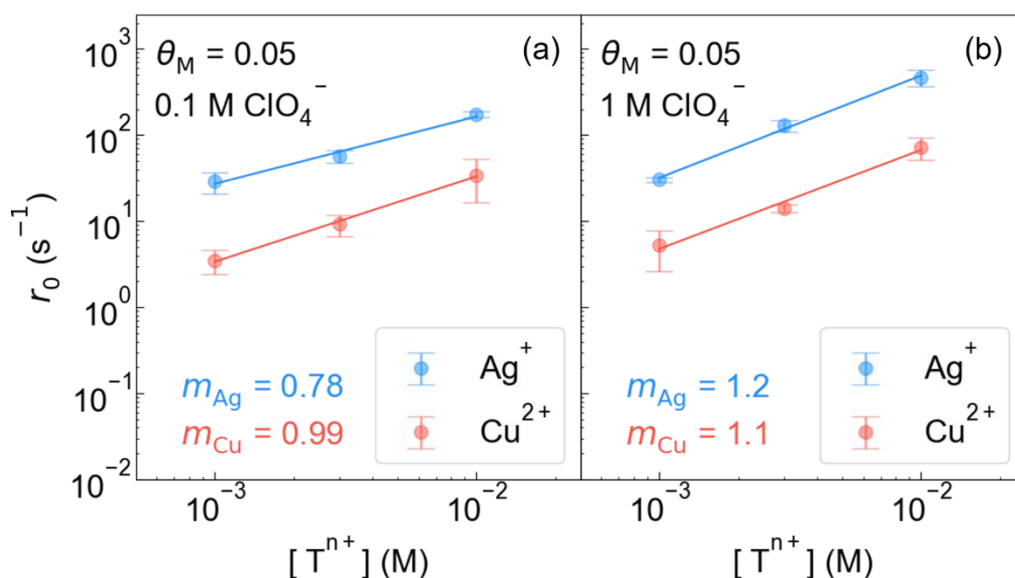


Figure 4: Equilibrium exchange rate (r_0) of metal cations versus the concentration of the respective metal cation ($[X] = 1.0 \text{ mM}$, 3.0 mM , 10.0 mM), measured at 5% coverage. (a) The exchange rates for Ag^+ (blue) and Cu^{2+} (orange) in 0.1 M ClO_4^- (b) The exchange rates for Ag^+ (blue) and Cu^{2+} (orange) in 1 M ClO_4^- . Circles represent experimental data, the error bars representing the standard deviation across three separate trials. The solid-colored lines represent the reaction order of the rates with respect to concentration. ($X = \text{Ag}^+$ or Cu^{2+}). The apparent reaction order, m , was measured from the slope $\partial \log(r_0) / \partial \log([X])$.



Figure 4 and Figure S10). **Figure 5** presents the trend in Cu^{2+} exchange rates for increasing supporting electrolyte concentrations. In solutions containing 1 mM Cu^{2+} , r_0 increased from 1.2 ± 0.5 to $14 \pm 0.1 \text{ s}^{-1}$ when the concentration of $\text{HClO}_4(\text{aq})$ increased from 0.010 to 10 M $\text{HClO}_4(\text{aq})$

(**Figure 5**). The m_{HClO_4} was 0.33, indicating that increased supporting electrolyte concentrations led to a moderate, positive impact on Cu^{2+} IIT kinetics. However, similar experiments in $\text{H}_2\text{SO}_4(\text{aq})$ electrolytes yielded increased r_0 at low $[\text{SO}_4^{2-}]$ and $m_{\text{H}_2\text{SO}_4}$ (0.05) was inconsistent with an electrolyte concentration effect, indicating that the identity of the supporting anion is dominant relative to H_3O^+ .

At increased concentrations of H_2SO_4 , the initial stages of Cu adsorption were no longer kinetically reversible, and a phase transition occurred prior to $\theta_{\text{Cu}} = 0.05$ (**Figure S11**).

The double layer structure for Au(111)/Cu

surfaces was studied by fitting the $\theta_{\text{Cu}}-E$ relationship for Cu^{2+} to adsorption isotherms for various $[\text{Cu}^{2+}]$ and $[\text{ClO}_4^-]$. Voltammetry data collected at $\nu = 25 \text{ mV s}^{-1}$ was sufficiently slow such that $E(\theta_{\text{Cu}})$ varied by less than 5 mV with a doubling of ν . These data were fit to a Frumkin $\theta-E$ isotherm

$$E = E_{1/2} + \frac{RT}{F} \left(-\ln[C_A]/n + \ln\left[\frac{\theta}{1-\theta}\right] + g\left[\theta - \frac{1}{2}\right] \right) \quad (5)$$

where $E_{1/2}$, R , F , C_A , n , and g are the potential of half coverage, the universal gas constant, Faraday's constant, bulk concentration of the dissolved transition metal, the number of charges per

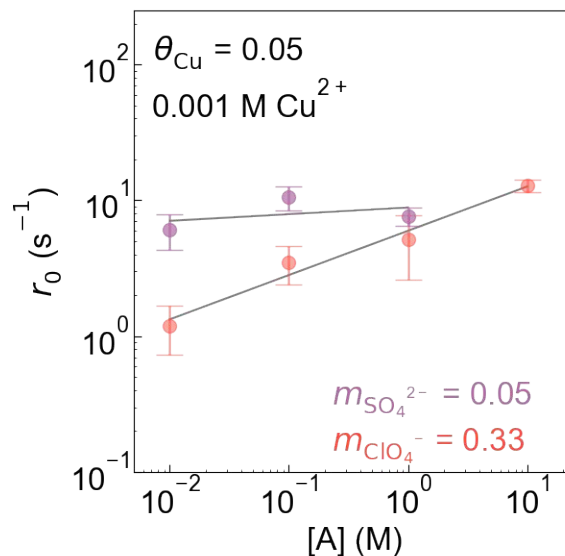


Figure 5: Dependence of the equilibrium exchange rate (r_0) of the metal cation vs the concentration of supporting anions ($[A]$) at 5% coverage. The light orange dots are perchlorate at $[\text{ClO}_4^-] = 0.01, 0.1, 1, 10 \text{ M}$. The purple dots are sulfate at $[\text{SO}_4^{2-}] = 0.01, 0.1, 1 \text{ M}$. The circle symbols represent experimental data, the error bars representing the standard deviations. The grey line represents the reaction order, m , with respect to supporting anion concentration.



adsorbate, and the adsorbate-adsorbate interaction parameter, respectively. A positive value for g indicates unfavorable adsorbate interactions and has been related to the free energy of interactions between adsorbed species, γ , by $g = 2\gamma/RT$.³² When g is zero, the equation for a potential-dependent Langmuir isotherm is recovered.

Cu^{2+} adsorbed onto Au(111) surfaces exhibited a positive g for all electrolytes studied in this work. In dilute (1.0 mM) Cu^{2+} and supporting electrolyte (10 mM ClO_4^-), g was 13 ± 4 (**Figure S12**) and decreased with increasing $[\text{ClO}_4^-]$ to 6.6 ± 0.6 and 2.9 ± 0.1 for 100 mM (**Figure S13**) and 1.00 M solutions (**Figure S14**), respectively. The average g for at least two independent measurements/electrode surfaces was generally insensitive to increasing $[\text{Cu}^{2+}]$ and varied from 2.9 to 3.6 in $[\text{ClO}_4^-] = 0.100$ M (**Figure S15**), although the apparent $E_{1/2}$ versus E_{rev} shifted positively up to 80 mV. Thus, although the interaction energies between adsorbed Cu^{2+} were insensitive to the bulk $[\text{Cu}^{2+}]$ (**Figure S15a**), they trended towards zero as the supporting electrolyte concentration was increased (**Figure S15b**).

It is possible that Ag^+ and Cu^{2+} promote adsorption by modifying the electric field more strongly than the supporting H_3O^+ cations,³³ and so we investigated the impact of supporting alkali cations via additions of K^+ to SO_4^{2-} electrolytes during adsorption of Cu^{2+} . Sulfate electrolytes were selected for this analysis because they conveniently lacked a strong anion concentration effect. The presence of K^+ led to an increased peak cathodic current relative to electrolytes where K^+ was absent (**Figure S16a**). K^+ had a substantial effect on the critical coverage of adsorbed Cu^{*z+} prior to the sharp current onset associated with a surface phase transition, however, K^+ did not appear to impact the θ - E behavior at more positive potentials compared to K-free electrolytes (**Figure S16b**). The exchange rate of Cu^{2+} at $\theta > 0.05$ and in the presence of K^+ was within experimental error of K^+ -free electrolytes (**Figure S17**).



Aqueous Cu^{2+} catalyzes the decomposition of ClO_4^- to Cl^- within weeks, and the presence of low concentrations ($<1 \mu\text{M}$) of Cl^- is likely to influence the kinetics of both Ag and Cu deposition.²⁵ To avoid any possible Cl^- contamination all Cu^{2+} solutions were tested within a week of preparation. A commensurate pair of minor, sharp peaks were noted in the reversible region of Cu^{2+} adsorption in aged $\text{Cu}(\text{ClO}_4)_2$ solutions (**Figure S18**), and we attribute these to the presence of Cl^- . Electrolytes which exhibited these peaks were considered to be Cl^- contaminated and were not used in the kinetic analysis.

Discussion:

Quasireversible adsorption of Ag and Cu on Au(111) electrodes allowed for direct measurements of interfacial ion transfer kinetics at a site-defined metal surface and in the absence of first-order phase transitions (**Figure 1**). Here, we have specifically focused on low (5%) coverages of adsorbates to maximize the contribution of isolated Au(111) adsorption sites to the measured faradaic response. Assuming that Ag and Cu were randomly distributed across three-fold hollow sites and that the contribution from step-edges and grain boundaries is negligible, the probability of the next adsorption site being free of nearest neighbor is $> 90\%$ when $\theta < 0.01$ but falls to $< 60\%$ when $\theta > 0.05$ (**Supplementary Information, S2**). Careful consideration and control of θ is thus essential for an atomistic understanding of metal IIT, and this quantity is rarely controlled during the deposition/corrosion of bulk metals. Measurements of UPD kinetics at low coverages may thus serve as a privileged model for site-specific charge transfer kinetics associated with these reactions. Similar adatoms are believed to be present during bulk deposition and corrosion. Gerischer reported the surface concentration of Ag adatoms to be $\sim 10^{13}/\text{cm}^2$, equivalent to 2–4% coverage, whereas Despic reported much greater concentrations of surface charge for Cu electrodes, equivalent to $\sim 3 \times 10^{15}/\text{cm}^2$, indicating the presence of a roughened surface and



hindering the ability to estimate the coverage of adsorbates.^{34,35} The reaction orders and turnover frequencies measured in this work are most pertinent to corrosion and deposition at low applied bias, when the coverage of adatoms is lowest.

The exchange rate for Ag at Au(111) is 2–6 times faster than the exchange rate for Cu independent of $[\text{Cu}^{2+}]$. The average standard rate constants for charge transfer, k^0 , are reported in **Table 1** and for Ag IIT in 1 M ClO_4^- are within one order of magnitude of some adiabatic electron transfer reactions ($0.85 \pm 0.2 \text{ cm s}^{-1}$).³⁶ The reported exchange rate for both Ag^+ and Cu^{2+} varies widely, presumably due to differences in surface preparation and the geometric density of active sites. Reported Cu^{2+} exchange current densities vary by an order of magnitude, from $0.4\text{--}4 \times 10^{-2} \text{ A cm}^{-2}$ in 5 mM CuSO_4 , with asymmetric transfer coefficients for the anodic and cathodic reactions.³⁷ Ag^+ exchange current densities vary wider still, based on electrode preparation and Ag^+ concentration, but the value measured here ($6 \times 10^{-3} \text{ A cm}^{-2}$) for elementary Ag IIT at 1 mM Ag^+ is slower than what has previously been reported for polycrystalline Ag surfaces ($1.5 \times 10^{-1} \text{ A cm}^{-2}$) at similar concentrations,^{38,39} suggesting that reported rates of Ag/Ag^+ exchange are convoluted by a large, albeit unknown, number of active sites. Here, we report a symmetric $\alpha = 0.5$ for elementary Cu^{2+} IIT, with a consistent standard rate constant of $1 \times 10^{-2} \text{ cm s}^{-1}$ at 5% surface coverage across varied electrolytes identities, ionic strengths, as well as $a_{\text{Cu}^{2+}}$. Notably, this value is within the range of reported rate constants for Cu^{2+} amalgamation ($1\text{--}5 \times 10^{-2} \text{ cm s}^{-1}$),⁴⁰ which serves as a similar model system for elementary IIT albeit where the concentration/surface excess of the adsorbed product is unknown.

Table 1: Comparison of standard rate constants for interfacial ion transfer of Ag^+ and Cu^{2+} at Au(111) in 0.10 M and 1 M HClO_4 at 20 °C.

k^0 (cm s ⁻¹) (0.10 M ClO_4^-)	k^0 (cm s ⁻¹) (1.00 M ClO_4^-)
---	---



Cu ²⁺	8(2) x 10 ⁻³	1.3(3) x 10 ⁻²
Ag ⁺	5.0(6) x 10 ⁻²	9.2(8) x 10 ⁻²

The reaction order for IIT exchange rates can be used to resolve microscopic steps associated with ion transfer. A unique aspect of adsorption/desorption reactions is that activity of the product cannot be controlled independently of the applied potential. Prior studies on adsorption at Pt(111) surfaces have reported a reaction order of 0.5 with respect to H₃O⁺ for hydride adsorption limited by proton-coupled-electron transfer, whereas the hydride adsorption from H₂O exhibits a 0th order dependence with respect to OH⁻ activity in alkaline media, implying that this process includes a chemically distinct rate determining step.²⁹ Both OH⁻ and H⁺ adsorption kinetics exhibit a stronger dependence on the concentration of supporting alkali cations, such as Na⁺, with $m_{\text{Na}^+} \sim 1$ reported for Pt(111) at pH ~ 13 . Here, we report that site-isolated transition metal, T, adsorption (eq 6)

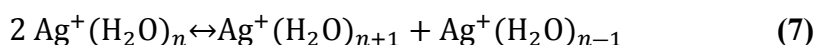


exhibits a consistent $\alpha \sim 0.5$ but $m \sim 2\alpha$ for both a monovalent and divalent transition metal cation. Generally, the measured m was ≥ 1 but for Ag⁺ adsorption in 0.10 M ClO₄⁻ and Cu²⁺ adsorption in 1.0 SO₄²⁻ m was 0.78 ± 0.09 and 0.8 ± 0.2 , respectively (**Figure 4, Figure S10**). We interpret these results to be generally consistent with, $m_{\text{T}^+} \sim 2\alpha$ and $0.4 < \alpha < 0.6$,³² which would be consistent with a single elementary charge transfer step but alludes to a more complex path for desolvation of aqueous transition metals (**Supplementary Information, S3–S8**).

The analysis for the self-exchange of Ag/Ag⁺, which does not require analysis of multiple charge transfer steps, provides a foundation for understanding metal IIT. The increased reaction order with respect to Ag⁺ is consistent with a general promoting effect of dissolved transition metal and this could be caused by specific intermolecular interactions or changes in the local electric



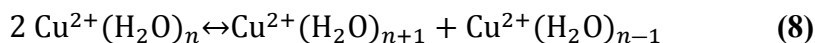
field at the adsorption site. For example, multi-step mechanisms that include a bimolecular reaction between $\text{Ag}^+(\text{aq})$ prior to the rate determining adsorption step may result in the measured $m_{\text{Ag}^+} = 2\alpha$ (e.g. $2 \text{Ag}^+ \leftrightarrow \text{Ag}_a^+ + \text{Ag}_b^+$) provided that the activity of both species are not linked by a simple mole balance. We hypothesize this step could be related to solvent exchange leading to an undercoordinated Ag^+ species which is able to more closely approach the adsorption site where charge transfer occurs (**equation 7, equations S20–S26**)



Previously calculated trajectories of individual Ag^+ deposition at model Ag surfaces indicate the presence of a pre-associated species within the inner Helmholtz plane, and later trajectories for Zn^{2+} deposition which include nonlinear solvent coupling terms further support an inner sphere pathway.^{12,41} In the case of silver, these results suggest that the formation of this species could be promoted by proximal, spectator Ag^+ cations. This case can easily be distinguished from a mechanism involving an adsorbed $\text{Ag}^{0/+}$ species acting as a promoter based on the coverage dependence of the reaction. However, the effects of pre-adsorption without charge transfer and the role of non-ideal interactions between adsorbates or the transition state are not distinguishable from the more general mechanism, based on differences in the exchange rate and transfer coefficient alone (**equations S27–S38**). The complex relationship between m_{T^+} and α may also be explained by transition metal cations exerting a generalized cation effect, by modifying the electric field at the site of transfer or by impacting the rigidity of the solvent within the double layer.⁴²

A similar analysis conducted for $\text{Cu}^{+/2+}$ exchange is consistent with the general presence of metal-cation promoted transfer which may be described by a bimolecular reaction prior to charge transfer, here represented as solvent exchange (**equation 8**).





We do not rule out the possibility of an alternate mechanism for metal cations to promote self-exchange, as a more comprehensive study of interactions with supporting metal cations is required. Although the reported $m_{\text{Cu}^{2+}}$ and α for Cu^{2+} vary widely based on electrolyte and electrode preparation,³⁷ Cu^{2+} deposition is generally believed to proceed via two distinct charge transfer steps, with the formation of unstable aqueous Cu^+ species being rate-determining. During these UPD measurements, outer-sphere electron transfer to Cu^{+2+} is unlikely, as the formal potential for the reaction is >200 mV negative of the electrochemical potentials used to quantify Cu^* exchange. Nevertheless, accounting for possible differences in the density of adsorption sites, the exchange currents measured for self-exchange of Cu^{2+} at Au(111) surfaces are generally in accord with previously reported values for overall Cu/Cu^{2+} exchange, suggesting that the coupled ion-electron transfer step quantified here, rather than homogeneous electron transfer to an aqueous Cu^{2+} species or chemical adsorption of Cu^{2+} prior to electron transfer, is an enabling step for the rapid kinetics of Cu deposition, generalized as **equation 9**.



Differences in the observed rate constant for Ag^+ adsorption and Cu^{2+} adsorption are more often attributed to chemical properties of the solvated metal cation, rather than the properties of the adsorbed $\text{Cu}^{0/+}$ or $\text{Ag}^{0/+}$ species. While the reorganization energy of the solvent is likely associated with a desolvation step, previously measured exchange rates for metal plating, as well as those measured here for IIT, are inconsistent with a transition state barrier that scales with the *total* solvation enthalpy.¹¹ Notably, despite a roughly four-fold difference between the solvation enthalpies of monovalent and divalent cations (5 eV and 20 eV respectively),^{12,18} the exchange rate of Ag^+ and Cu^{2+} at Au(111) differ only by a factor of two in 0.10 M HClO_4 . This suggests that



the bulk solvation enthalpy is a poor descriptor for the reorganization energy associated with the rate determining step of transition metal IIT. This data strengthens the argument that most of the enthalpy of desolvation associated with a metal deposition or corrosion reaction occurs before/after the rate determining step. The approach distance of the monovalent cation is expected to be less than that of the divalent cation, as calculated for Zn^{2+} and Zn^+ at Zn metal surfaces,¹⁶ but this apparently does not directly influence the apparent α . Inspired by recent simulations of Zn/ Zn^{2+} deposition, we hypothesize that the greater approach distance for the solvated Cu^{2+} species leads to weaker coupling and the more sluggish IIT kinetics in comparison to Ag^+ .⁴³

The weakly positive correlation between IIT kinetics and increasing perchloric acid concentration is consistent with either increased screening effects in the double layer and/or decreasing rigidity of the double layer with increasing ionic strength.³⁰ Near-surface anions support a greater surface excess of cations and thereby increase the local concentration of reactants prior to desolvation and ion transfer. These effects are also evident in the θ - E response, which provides surface-sensitive information about changes to the adsorbate environment in response to changes in the bulk electrolyte (**Figure S15b**). The apparent g for adsorbed Cu at Au(111) was insensitive to the concentration of Cu^{2+} but was weakly influenced by the concentration of $HClO_4$, indicating less repulsive interactions between surface cations. A decrease in g could be caused by a combination of increased screening effects with higher ionic strength and/or the increased anion concentration disrupting interactions between interfacial water.³⁰

Whereas perchlorate lacks an ordered adsorption phase and exhibits a lower capacitance in the potential window used for kinetic analysis (**Figure S19**), sulfate anions form an ordered layer ($\theta = 0.2$) on Au(111),^{44,45} and a disordered layer has been observed at concentrations > 5 M.⁴⁶ The zeroth-order anion effect for sulfate at Au(111), stands in contrast to the positive anion effect for



perchlorate, and is consistent with a relatively stable Γ_{SO_4} with increasing $a_{\text{H}_2\text{SO}_4}$ for $\text{pH} \geq 0$. The presence of K^+ in sulfate-containing electrolytes did not lead to a change in the apparent interaction parameter at low coverages. However, K^+ cations did contribute to a positive shift in the peak potential which was caused by a lesser integrated charge prior to the sharp change in current assigned to a surface phase transition (**Figure S16b**). This suggests that although K^+ cations do not impact the stability of Cu adsorbates at low coverages, they induce a transition to an ordered surface layer at a lower Cu coverage, likely because they contribute to the total excess charge within the double layer region.

No differences in metal IIT were observed in response to a change in the bulk $a_{\text{H}_2\text{O}}$. The activity of water in 10 M $\text{HClO}_4(\text{aq})$ and 10 M $\text{H}_2\text{SO}_4(\text{aq})$ is 0.03 and 0.045, respectively,^{47,48} but the exchange rate for Cu^{2+} was consistent across a wide range of $[\text{H}_2\text{SO}_4]$ and exhibited a similar m_{HClO_4} at low and high concentrations. Uncoordinated water is a necessary product of the overall deposition of aqueous transition metals, and this result implies that either the surface activity of H_2O is relatively insensitive to changes in the bulk activity or else uncoordinated H_2O is not a participant in the rate determining step for Cu^{2+} IIT. This is significant for understanding the behavior of metal plating and ion insertion reactions in “water-in-salt” electrolytes and suggests that there is a significant barrier to modifying the solvent activity without changes to the electrode surface environment itself.^{49,50}

A few experimental barriers to measuring isolated steps of deposition/corrosion have been mitigated here through the use of freshly prepared Au(111) surfaces and Cu^{2+} electrolytes prepared from high purity oxides. Investigations of Ag UPD at Au surfaces have previously been limited in part due to the tendency of Ag to alloy with the substrate, leading to a time-varying and irreproducible electrochemical response.²³ Au(111) surfaces exhibited changes in electrochemical



response after less than 30 min of exposure (**Figure 1c**), whereas frequent replacement of Au(111)-textured thin film electrodes allowed for reproducible measurements of Ag desorption kinetics without the apparent influence of Ag/Au surface alloys that would not be possible with traditional Au(111) solid electrodes (**Figure 4**). The positive shift in the Ag desorption peak implies more favorable Ag/Au interactions that could be caused by an increase in vacancies, pits, step edges serving as active sites. As the extent of Ag/Au alloying increases, the number of active sites for Ag UPD decreases, which would lead to an overestimation of the active sites and underestimation of the apparent rate and exchange rate. Furthermore, the electronic properties of the adsorption sites will be modified after the formation of a near-surface alloy and this could be reflected in the changing onset potential for desorption (**Figure 1c**).

Future studies of metal IIT should investigate the chemical principles required to predict rate constants for metal adsorption, including the electronic structure of metal cations and the coordination environment of the adsorption site. Studies on the temperature dependence and supporting cation identity may further clarify how solvent transfer and reorganization influence the rate of IIT, which would provide design principles for accelerated deposition or suppressed corrosion. Additionally, the methodology to measure exchange rates for controlled metal adsorbates could shed light on the molecular mechanisms of additives used for Cu deposition in semiconductor interconnects, increasing charge/discharge rates in redox-flow battery electrolytes, and the industrial electrowinning and electrorefining process of energy-critical metals.

Conclusions:

Underpotential deposition of Cu^{2+} and Ag^+ at well-defined Au(111) interfaces served to isolate a microscopically reversible step involved in metal corrosion and deposition and enabled a controlled kinetic analysis of self-exchange during interfacial ion transfer. This system addresses



two limitations of traditional kinetic measurements at growing/corroding metal surfaces: (1) the coverage of adsorbates is not known and (2) both the number density and identity of active sites are poorly defined. The standard rate constant for Ag^+ IIT at Au(111) was within an order of magnitude of the reported adiabatic electron transfer for $\text{Ru}(\text{NH}_3)_6$ and the exchange rate of Cu^{2+} was consistently within an order of magnitude of that measured for Ag^+ . The coverage dependence and transfer coefficient associated with adsorption/desorption of both Ag^+ and Cu^{2+} suggests that a coupled ion-electron transfer step was the rate determining step for adsorption/desorption. The self-exchange rate with respect to the metal cation concentration was quantified at constant coverage of adsorbates and was ~ 1 for both Cu^{2+} and Ag^+ ; this could be described by a multi-step mechanism involving biomolecular interactions between free cations prior to transfer. A mechanism involving solvent transfer prior to adsorption/desorption was proposed to fit this mechanism and is consistent with zeroth-order kinetics with respect to bulk H_2O . A positive anion effect was observed in perchlorate but not in sulfate electrolytes, with the latter exhibiting increased exchange rates at lower ionic strengths.

Author contributions:

E.I.S. Conceptualization, methodology, investigation, visualization, writing – original draft, review, & editing; **K.A.T.** methodology, investigation, visualization, writing – review & editing; **F.B.S.** investigation, writing – review & editing; **P.A.K.** supervision, visualization, writing – original draft, review, & editing

Conflicts of interest:

There are no conflicts to declare

Data availability:



Additional data supporting this article have been included as part of the Supplementary Information: **equations S1-S56, Figures S1-S19, Table S1**, a detailed derivation of kinetic models, x-ray diffraction of annealed Au thin films, high resolution XPS data for annealed Au electrodes before and after exposure to Ag⁺, additional electrochemical data and measured exchange rates in concentrated H₂SO₄ and solutions containing K⁺. Unprocessed electrochemical data is available at <https://github.com/Kempler-Group/CuAgUPD2026> (a permalink will be created prior to publication)

Acknowledgements:

This material is based on work performed by the Liquid Sunlight Alliance, which is supported by the U.S. Department of Energy, Office of Science, Office of Basic Energy Sciences, Fuels from Sunlight Hub under Award Number DE-SC0021266. We thank Shannon W. Boettcher and Jin Suntivich for valuable scientific discussions on interfacial ion transfer kinetics.

Notes and references:

- (1) Andricacos, P. C.; Uzoh, C.; Dukovic, J. O.; Horkans, J.; Deligianni, H. Damascene Copper Electroplating for Chip Interconnections. *IBM J. Res. Dev.* **1998**, *42* (5), 567–574. <https://doi.org/10.1147/rd.425.0567>.
- (2) Jhothiraman, J. K.; Balachandran, R. Electroplating: Applications in the Semiconductor Industry. *Adv. Chem. Eng. Sci.* **2019**, *9* (2), 239–261. <https://doi.org/10.4236/aces.2019.92018>.
- (3) *Copper Plating Solutions for Semiconductor Manufacturing Market Growth Analysis, Market Dynamics, Key Players and Innovations, Outlook and Forecast 2025-2031- Intelmarketresearch*. <https://www.intelmarketresearch.com/chemicals-and-materials/375/copper-plating-solutions-semiconductor> (accessed 2025-04-17).
- (4) Gileadi, E. Problems in Interfacial Electrochemistry That Have Been Swept under the Carpet. *J. Solid State Electrochem.* **2011**, *15* (7–8), 1359–1371. <https://doi.org/10.1007/s10008-011-1344-5>.
- (5) Lewis, N. B.; Kelly, J.; Gardner, J. G.; Razdan, N. K.; Ardo, S.; Markland, T. E.; Surendranath, Y. Ion-Exchange-Mediated Pre-Association Gates Interfacial PCET. *Chem* **2025**, *0* (0). <https://doi.org/10.1016/j.chempr.2025.102813>.
- (6) D'Antona, N.; Kelly, J.; Barnard, N.; Ardo, S.; Wang, Y.; Surendranath, Y.; Markland, T. E.; Kempler, P. A.; Boettcher, S. W. Proton-Transfer Kinetics at Liquid–Liquid Interfaces. *J. Am. Chem. Soc.* **2025**, *147* (25), 21408–21418. <https://doi.org/10.1021/jacs.4c18349>.



- (7) Tang, D.; Keyes, N.; Rose, J. C.; Gonzales, J. E.; Yang, M.; Giles, M. D.; Surendranath, Y.; Ardo, S.; Minus, M. B. Synthesis of 4,5-Disubstituted *o*-Phenylenediamines: An Enabling Platform for Electrochemical Investigations of Interfacial Ion Transfer Reactions. *J. Org. Chem.* **2025**, acs.joc.5c00538. <https://doi.org/10.1021/acs.joc.5c00538>.
- (8) Zhang, Y.; Fraggedakis, D.; Gao, T.; Pathak, S.; Zhuang, D.; Grosu, C.; Samantaray, Y.; Neto, A. R. C.; Duggirala, S. R.; Huang, B.; Zhu, Y. G.; Giordano, L.; Tatara, R.; Agarwal, H.; Stephens, R. M.; Bazant, M. Z.; Shao-Horn, Y. Lithium-Ion Intercalation by Coupled Ion-Electron Transfer. *Science* **2025**, 390 (6768), eadq2541. <https://doi.org/10.1126/science.adq2541>.
- (9) Chidsey, C. E. D. Free Energy and Temperature Dependence of Electron Transfer at the Metal-Electrolyte Interface. *Science* **1991**, 251 (4996), 919–922. <https://doi.org/10.1126/science.251.4996.919>.
- (10) Conway, B. E.; Bockris, J. O. The Mechanism of Electrolytic Metal Deposition. *Proc. R. Soc. Lond. Ser. Math. Phys. Sci.* **1997**, 248 (1254), 394–403. <https://doi.org/10.1098/rspa.1958.0251>.
- (11) Gileadi, E. The Enigma of Metal Deposition. *J. Electroanal. Chem.* **2011**, 660 (2), 247–253. <https://doi.org/10.1016/j.jelechem.2011.01.025>.
- (12) Pinto, L. M. C.; Spohr, E.; Quaino, P.; Santos, E.; Schmickler, W. Why Silver Deposition Is so Fast: Solving the Enigma of Metal Deposition. *Angew. Chem. Int. Ed.* **2013**, 52 (30), 7883–7885. <https://doi.org/10.1002/anie.201301998>.
- (13) Kang, R.; Zhao, Y.; Hait, D.; A. Gauthier, J.; A. Kempler, P.; A. Thurman, K.; W. Boettcher, S.; Head-Gordon, M. Understanding Ion-Transfer Reactions in Silver Electrodeposition and Electrodeposition from First-Principles Calculations and Experiments. *Chem. Sci.* **2024**, 15 (13), 4996–5008. <https://doi.org/10.1039/D3SC05791G>.
- (14) Darvas, M.; Jorge, M.; Cordeiro, M. N. D. S.; Kantorovich, S. S.; Sega, M.; Jedlovszky, P. Calculation of the Intrinsic Solvation Free Energy Profile of an Ionic Penetrant Across a Liquid–Liquid Interface with Computer Simulations. *J. Phys. Chem. B* **2013**, 117 (50), 16148–16156. <https://doi.org/10.1021/jp404699t>.
- (15) Clabaut, P.; Schweitzer, B.; Götz, A. W.; Michel, C.; Steinmann, S. N. Solvation Free Energies and Adsorption Energies at the Metal/Water Interface from Hybrid Quantum-Mechanical/Molecular Mechanics Simulations. *J. Chem. Theory Comput.* **2020**, 16 (10), 6539–6549. <https://doi.org/10.1021/acs.jctc.0c00632>.
- (16) Pecina, O.; Schmickler, W. The Solvent Influence on the Electrochemical Transfer of Divalent Ions. *Chem. Phys.* **2000**, 252 (3), 349–357. [https://doi.org/10.1016/S0301-0104\(99\)00332-8](https://doi.org/10.1016/S0301-0104(99)00332-8).
- (17) Pecina, O.; Schmickler, W.; Spohr, E. On the Mechanism of Electrochemical Ion Transfer Reactions. *J. Electroanal. Chem.* **1995**, 394 (1–2), 29–34. [https://doi.org/10.1016/0022-0728\(95\)92838-O](https://doi.org/10.1016/0022-0728(95)92838-O).
- (18) Uudsemaa, M.; Tamm, T. Calculation of Hydration Enthalpies of Aqueous Transition Metal Cations Using Two Coordination Shells and Central Ion Substitution. *Chem. Phys. Lett.* **2004**, 400 (1), 54–58. <https://doi.org/10.1016/j.cplett.2004.10.082>.
- (19) Hölzle, M. H.; Zwing, V.; Kolb, D. M. The Influence of Steps on the Deposition of Cu onto Au(111). *Electrochimica Acta* **1995**, 40 (10), 1237–1247. [https://doi.org/10.1016/0013-4686\(95\)00055-J](https://doi.org/10.1016/0013-4686(95)00055-J).



- (20) Hölzle, M. H.; Retter, U.; Kolb, D. M. The Kinetics of Structural Changes in Cu Adlayers on Au(111). *J. Electroanal. Chem.* **1994**, *371* (1), 101–109. [https://doi.org/10.1016/0022-0728\(93\)03235-H](https://doi.org/10.1016/0022-0728(93)03235-H).
- (21) Herrero, E.; Buller, L. J.; Abruña, H. D. Underpotential Deposition at Single Crystal Surfaces of Au, Pt, Ag and Other Materials. *Chem. Rev.* **2001**, *101* (7), 1897–1930. <https://doi.org/10.1021/cr9600363>.
- (22) Herrero, E.; Abruña, H. D. Underpotential Deposition of Mercury on Au(111): Electrochemical Studies and Comparison with Structural Investigations. *Langmuir* **1997**, *13* (16), 4446–4453. <https://doi.org/10.1021/la970109t>.
- (23) Whelan, C. M.; Smyth, M. R.; Barnes, C. J.; Attard, G. A.; Yang, X. Surface Structural Transitions Induced by Repetitive Underpotential Deposition of Ag on Au(111). *J. Electroanal. Chem.* **1999**, *474* (2), 138–146. [https://doi.org/10.1016/S0022-0728\(99\)00320-4](https://doi.org/10.1016/S0022-0728(99)00320-4).
- (24) Krznarić, D.; Goričnik, T. Reactions of Copper on the Au(111) Surface in the Underpotential Deposition Region from Chloride Solutions. *Langmuir* **2001**, *17* (14), 4347–4351. <https://doi.org/10.1021/la001562z>.
- (25) Hotlos, J.; Magnussen, O. M.; Behm, R. J. Effect of Trace Amounts of Cl⁻ in Cu Underpotential Deposition on Au(111) in Perchlorate Solutions: An in-Situ Scanning Tunneling Microscopy Study. *Surf. Sci.* **1995**.
- (26) Ogaki, K.; Itaya, K. In Situ Scanning Tunneling Microscopy of Underpotential and Bulk Deposition of Silver on Gold (111). *Electrochimica Acta* **1995**, *40* (10), 1249–1257. [https://doi.org/10.1016/0013-4686\(95\)99706-2](https://doi.org/10.1016/0013-4686(95)99706-2).
- (27) Park, I.; Baltruschat, H. In Situ Friction Study of Ag Underpotential Deposition (UPD) on Au(111) in Aqueous Electrolyte. *ChemPhysChem* **2021**, *22* (10), 952–959. <https://doi.org/10.1002/cphc.202100130>.
- (28) Nehal, M. El. F.; Bouzidi, A.; Nakrela, A.; Miloua, R.; Medles, M.; Desfeux, R.; Blach, J.-F.; Simon, P.; Huvé, M. Synthesis and Characterization of Antireflective Ag@AgCl Nanocomposite Thin Films. *Optik* **2020**, *224*, 165568. <https://doi.org/10.1016/j.ijleo.2020.165568>.
- (29) Kuo, D.-Y.; Lu, X.; Hu, B.; Abruña, H. D.; Suntivich, J. Rate and Mechanism of Electrochemical Formation of Surface-Bound Hydrogen on Pt(111) Single Crystals. *J. Phys. Chem. Lett.* **2022**, *13* (27), 6383–6390. <https://doi.org/10.1021/acs.jpcclett.2c01734>.
- (30) Lin, C.-Y.; Abruña, H. D.; Suntivich, J. Cations Affect Water Activation on Pt(111) in Alkaline Media. *J. Electrochem. Soc.* **2025**, *172* (1), 016503. <https://doi.org/10.1149/1945-7111/ada7a3>.
- (31) Thurman, K. A.; Cannan, C. M.; Shekhar, R.; Zhao, Y.; Boettcher, S. W.; Kempler, P. A. Anions in Corrosion: Influence of Polymer Electrolytes on the Interfacial Ion Transfer Kinetics of Cu at Au(111) Surfaces. *ACS Electrochem.* **2025**. <https://doi.org/10.1021/acselectrochem.4c00181>.
- (32) Bard, A. J.; Faulkner, L. R.; White, H. S. Electrochemical Methods.
- (33) Monteiro, M. C. O.; Dattila, F.; Hagedoorn, B.; Garcia-Muelas, R.; Lopez, N.; Koper, M. T. M. Absence of CO₂ Electroreduction on Copper, Gold and Silver Electrodes without Metal Cations in Solution. *Nature Catalysis*, **2021**, *4*, 654–662.
- (34) Despić, A. R. Deposition and Dissolution of Metals and Alloys. Part B: Mechanisms, Kinetics, Texture, and Morphology. In *Comprehensive Treatise of Electrochemistry: Volume 7 Kinetics and Mechanisms of Electrode Processes*; Conway, B. E., Bockris, J. O., Yeager,



- E., Khan, S. U. M., White, R. E., Eds.; Springer US: Boston, MA, 1983; pp 451–528. https://doi.org/10.1007/978-1-4613-3584-9_8.
- (35) Gerischer, H. Zum Mechanismus Der Elektrolytischen Abscheidung Und Auflösung Fester Metalle II. Galvanostatische Einschaltvorgänge an Silberelektroden Und Die Kinetik Des Kristallwachstums. *Z. Für Elektrochem. Berichte Bunsenges. Für Phys. Chem.* **1958**, *62* (3), 256–264. <https://doi.org/10.1002/bbpc.19580620308>.
- (36) Santos, E.; Iwasita, T.; Vielstich, W. On the Use of the Coulostatic Method for the Investigation of Fast Redox Systems. *Electrochimica Acta* **1986**, *31* (4), 431–437. [https://doi.org/10.1016/0013-4686\(86\)80105-0](https://doi.org/10.1016/0013-4686(86)80105-0).
- (37) Despić, A. R. Deposition and Dissolution of Metals and Alloys. Part B: Mechanisms, Kinetics, Texture, and Morphology. In *Comprehensive Treatise of Electrochemistry*; Conway, B. E., Bockris, J. O., Yeager, E., Khan, S. U. M., White, R. E., Eds.; Springer US: Boston, MA, 1983; pp 451–528. https://doi.org/10.1007/978-1-4613-3584-9_8.
- (38) Gerischer, H. Models for the Discussion of the Photo-Electrochemical Response of Oxide Layers on Metals. *Corrosion Science*, 1989, *29*, 257–266.
- (39) Larkin, D.; Hackerman, N. The Ag⁺-Ag Exchange Reaction in Aqueous Acidic Nitrate Electrolyte. *J. Electrochem. Soc.* **1977**, *124* (3), 360.
- (40) Randles, J. E. B.; Somerton, K. W. Kinetics of Rapid Electrode Reactions. Part 4.—Metal Ion Exchange Reaction at Amalgam Electrodes. *Trans. Faraday Soc.* **1952**, *48*, 951–955.
- (41) Quaino, P.; Colombo, E.; Juarez, F.; Santos, E.; Belletti, G.; Groß, A.; Schmickler, W. On the First Step in Zinc Deposition – A Case of Nonlinear Coupling with the Solvent. *Electrochem. Commun.* **2021**, *122*, 106876. <https://doi.org/10.1016/j.elecom.2020.106876>.
- (42) Resasco, J. A Universal Model of Cation Effects in Electrocatalysis. *JACS Au* **2025**, *5* (11), 5253–5266. <https://doi.org/10.1021/jacsau.5c01115>.
- (43) Quaino, P.; Colombo, E.; Juarez, F.; Santos, E.; Belletti, G.; Groß, A.; Schmickler, W. On the First Step in Zinc Deposition – A Case of Nonlinear Coupling with the Solvent. *Electrochem. Commun.* **2021**, *122*, 106876. <https://doi.org/10.1016/j.elecom.2020.106876>.
- (44) Hausen, F.; Gosvami, N. N.; Bennewitz, R. Anion Adsorption and Atomic Friction on Au(111). *Electrochimica Acta* **2011**, *56* (28), 10694–10700. <https://doi.org/10.1016/j.electacta.2011.03.013>.
- (45) Edens, G. J.; Gao, X.; Weaver, M. J. The Adsorption of Sulfate on Gold(111) in Acidic Aqueous Media: Adlayer Structural Inferences from Infrared Spectroscopy and Scanning Tunneling Microscopy.
- (46) Sato, K.; Yoshimoto, S.; Inukai, J.; Itaya, K. Effect of Sulfuric Acid Concentration on the Structure of Sulfate Adlayer on Au(111) Electrode. *Electrochem. Commun.* **2006**, *8* (5), 725–730. <https://doi.org/10.1016/j.elecom.2006.03.001>.
- (47) Karelin, A. I.; Tarasenko, V. A. The Water Activity and Free Water Mole Fraction in Perchloric Acid. *J. Solut. Chem.* **2015**, *44* (1), 146–151. <https://doi.org/10.1007/s10953-014-0285-x>.
- (48) Zhang, L.; Grace, P. M.; Sun, D.-W. An Accurate Water Activity Model for Sulfuric Acid Solutions and Its Implementation on Moisture Sorption Isotherm Determination. *Dry. Technol.* **2022**, *40* (12), 2540–2549. <https://doi.org/10.1080/07373937.2020.1869037>.
- (49) Zhao, Y.; Hu, X.; Stucky, G. D.; Boettcher, S. W. Thermodynamic, Kinetic, and Transport Contributions to Hydrogen Evolution Activity and Electrolyte-Stability Windows for Water-in-Salt Electrolytes. *J. Am. Chem. Soc.* **2024**, *146* (5), 3438–3448. <https://doi.org/10.1021/jacs.3c12980>.



- (50) Suo, L.; Borodin, O.; Gao, T.; Olguin, M.; Ho, J.; Fan, X.; Luo, C.; Wang, C.; Xu, K. “Water-in-Salt” Electrolyte Enables High-Voltage Aqueous Lithium-Ion Chemistries. *Science* **2015**, *350* (6263), 938–943. <https://doi.org/10.1126/science.aab1595>.



Data availability:

Additional data supporting this article have been included as part of the Supplementary Information: **equations S1-S56, Figures S1-S19, Table S1**, a detailed derivation of kinetic models, x-ray diffraction of annealed Au thin films, high resolution XPS data for annealed Au electrodes before and after exposure to Ag^+ , additional electrochemical data and measured exchange rates in concentrated H_2SO_4 and solutions containing K^+ . Unprocessed electrochemical data is available at <https://github.com/Kempler-Group/CuAgUPD2026> (a permalink will be created prior to publication)

